Journal of Biomechanics 119 (2021) 110327

Contents lists available at ScienceDirect

Journal of Biomechanics

journal homepage: www.elsevier.com/locate/jbiomech
www.JBiomech.com

Aerodynamic investigation of tucked positions in alpine skiing

Ola Elfmark [a,*], Knut Erik Teigen Giljarhus [b], Fredrik Fang Liland [c], Luca Oggiano [c], Robert Reid [d]

[a] Norwegian University of Science and Technology, Department of Civil and Environmental Engineering, N-7491 Trondheim, Norway
[b] University of Stavanger, Department of Mechanical and Structural Engineering and Materials Science, 4068 Stavanger, Norway
[c] Nabla Flow AS, Stavanger, Norway
[d] Norwegian Ski Federation, Oslo, Norway

ARTICLE INFO

Article history:
Accepted 8 February 2021

Keywords:
Sports aerodynamics
Alpine skiing
Wind tunnel
Computational Fluid Dynamics

ABSTRACT

The purpose of this investigation was to examine the aerodynamics of tucked positions in competitive alpine skiing. To further our understanding of how a skier's position affects the air flow and the resulting aerodynamic drag, a combination of both experimental and simulation methods was used. This study focused in particular on the effect of skier torso and thigh angles relative to the air flow direction, as these two angles have been previously found to be important determinants of aerodynamic performance in tucked positions. Two top 30 world-ranked skiers were investigated in two different wind tunnels, and the results were compared with Computational Fluid Dynamics (CFD) simulations performed using a 3D scan of one of the athlete. To quantify the effect of torso and thigh angles on skier drag, changes in drag were measured relative to baseline positions.

Skier drag area increased by approximately 0.8 and 1.2% per degree increase in torso and thigh angles relative to the baseline position, respectively. This trend was consistent between both of the experimental wind tunnel tests as well as the CFD simulations, indicating good agreement between methods. The CFD simulations further indicated that the air flow about the lower legs made the largest contribution to skier drag, accounting for as much as 40–50% of the total drag area in low tuck positions. Based on these findings, a low tuck position where the torso angle approaches 0° and the knees help to fill the gap behind the armpits will minimize skier aerodynamic drag.

1. Introduction

The performance time of an alpine ski racer is, on a fundamental level, a function of the skier's speed and trajectory, both of which are determined by the balance of external forces acting on the skier. These include gravity, the reaction force from the snow surface, and aerodynamic drag. Particularly in the high-speed disciplines of Downhill (DH) and Super-G (SG) where speeds can reach as high as 35–40 ms^{-1}, the aerodynamic drag force can account for as much as 80–90% of the total resistive force acting on a skier (Savolainen and Visuri, 1994). As such, any reduction in aerodynamic drag can have a significant impact on performance. The drag force acting on an alpine skier can be formulated as

$$F_D = \frac{1}{2}\rho V^2 C_D A, \quad (1)$$

where ρ is the density of air, V the relative velocity, C_D the drag coefficient and A the frontal area of the skier. The influence of F_D, relative to other forces, will increase with speed as $F_D \propto V^2$. The drag coefficient is dependent on the Reynolds number, surface roughness and the skier's shape. Experimental results in studies of athlete aerodynamics are often presented as the product of the drag coefficient and frontal area, known as the drag area (C_DA) (Meyer et al., 2012; Brownlie, 2020). The most common approach used to study skier aerodynamics has been wind tunnel testing. In 1977, Watanabe and Ohtsuki (1977) published one of the first wind tunnel experiments measuring the aerodynamic forces acting on an alpine skier. Wind tunnel testing has subsequently been used as a method in numerous studies (Barelle et al., 2004; Brownlie et al., 2010; Meyer et al., 2012; Supej et al., 2013; Elfmark and Bardal, 2018; Elfmark et al., 2020). Performing wind tunnel measurements can give accurate measurements of the drag force, but it is both time consuming and expensive to perform.

Due to rapid technological developments in recent years, Computational Fluid Dynamics (CFD) has evolved into a method to study aerodynamics in its own right, complementing many of the limitations seen in wind tunnel testing. For instance, by using CFD, one can predict and visualize the flow field around an object

* Corresponding author.
E-mail address: ola.elfmark@ntnu.no (O. Elfmark).

https://doi.org/10.1016/j.jbiomech.2021.110327
0021-9290/

as well as estimate the pressure distribution and drag information of individual body segments. However, simplifications in the simulations are often necessary to reduce computational cost. CFD has been extensively used in other sports such as cycling (Oggiano et al., 2015; Defraeye et al., 2010; Blocken et al., 2013; Blocken and Toparlar, 2015; Blocken et al., 2016; Giljarhus and Stave, 2020) and ski jumping (Gardan et al., 2017; Meile et al., 2006; Nørstrud and Øye, 2009), but has only rarely been used in alpine skiing. In one notable exception, Chen and Fang (2011) investigated the effect of wind and posture on aerodynamic performance during the flight phase of a jump in alpine skiing by using a 2D CFD flow simulation. They showed that the skier's posture during jump flight had a significant impact on drag, however the assumption of a 2D geometry limits the study's applicability. In a second example, Asai et al. (2016) used CFD to characterize the relationship between the flow velocity and drag force of a typical low tuck position, and compared the results with wind tunnel measurements. They identified the head, upper arms, thighs, and lower legs as the main sources of drag, with the lower legs accounting for as much as 40% of the total drag acting on the skier.

Although tucked positions are frequently used in competition to reduce drag, the mechanisms affecting drag in these positions are not well understood. While significant resources are invested at the professional level to study how a skier's position affects drag, relatively little of this knowledge is published in the scientific literature thus limiting our understanding. One purpose of this paper is therefore to report findings of an investigation done at the elite level in Norway to examine factors influencing drag in tuck positions. Given the complementary nature of the strengths and weaknesses of wind tunnel testing and CFD methods, both approaches were used in conjunction to provide greater insight into the mechanisms affecting skier drag.

2. Methods

To take advantage of the complementary nature of wind tunnel and CFD methods, this study was divided into two parts. In the first part, two elite skiers were tested in a selection of low tuck positions and variations of these positions in two different wind tunnels. In the second part, a 3D scans of one of the skiers in low tuck positions was later used to generate a "digital twin" whose positions could be modified to investigate similar trends observed in the wind tunnel testing using CFD.

2.1. Experimental setup

2.1.1. Subjects

One female and one male alpine skier, both top 30 world-ranked, from the Norwegian national team participated in the study. Prior to formally giving their consent, both participants were informed of the study's purpose, benefits, and potential risks, as well as their right to withdraw from the study at any time. The study was conducted in accordance with the Declaration of WMA (2001).

2.1.2. Wind tunnel setup

The two wind tunnel experiments were performed at the Norwegian University of Science and Technology (E1) and at the Politecnico di Milano high speed wind tunnel (E2). The main characteristics for both wind tunnels are reported in Appendix A. In both investigations, alpine bindings were mounted onto the force balance and cameras were positioned outside the wind tunnel to film the skiers from a side-view perspective. Live video feed from the side-view was shown on a screen mounted into the floors of both wind tunnels. To assist athletes in finding test positions, graphical cues were superimposed onto the live video feed.

2.1.3. Wind tunnel test protocol

In E1, the air flow speed was set to 25 ms^{-1}, the maximum capacity for this wind tunnel. As this speed is somewhat lower than that characteristic of DH and SG, the experiment was repeated at E2 at 30 ms^{-1} for the female and 35 ms^{-1} for the male athlete. Three measurements were made for each test position with 20 s sampling time. Images from the side-view camera taken at the start and finish of each trial were used to both verify that the intended position was maintained throughout the sampling period as well as to measure skier torso and thigh angles. Torso (θ_1) and thigh (θ_2) angles relative to the air flow were measured by manually digitizing the knee joint center, hip joint center and head center of mass (Fig. 1). To estimate angle measurement uncertainty, 10 pictures were measured 10 times each. The standard error of these repeated measurements was ± 0.9 °.

Prior to wind tunnel testing, a baseline position was defined for each athlete as their typical low tuck position they would use in competition. This position, which was measured at the start of each parameter test, was to serve as a common reference for studying relative trends in drag development for each test. A parameter test consisted of an initial baseline position measurement followed by a series of measurements with systematically increased torso or thigh angles. The effects of torso and thigh angle were tested independently throughout what was considered a realistic range of motion. An angle was considered to be at an extreme when the athlete could no longer increase or decrease the angle without changing the rest of their posture due to anatomical constraints. Torso angle θ_1 and thigh angle θ_2 for the investigated positions ranged from 0–30 ° and 30–60 °, respectively. To help illustrate, Fig. 1 shows a selection of the investigated positions for both athletes as well as the CFD model.

2.2. Computational setup

The female athlete was scanned in the baseline position using an Artec Eva scanner and the resulting geometry model was post-processed with the Artec Studio 14 software. To test the effect of skier torso and thigh angles, digital morphing was applied to the 3D skier model to systematically and independently adjust these angles from the scanned baseline position, in a manner similar to the wind tunnel experiments. Fig. 1(b) and (e) shows the model for the baseline position and the morphed model for the position with the highest simulated torso angle θ_1, respectively. The simulations were performed in the open-source CFD simulation software OpenFOAM, version 7 (Weller et al., 1998; Jasak et al., 2007). Details of the computational set-up are provided in Appendix B.

The total C_DA was calculated with the following formula:

$$C_DA = \frac{2}{\rho V_{rel}^2}\left(\underbrace{\iint_S p \cdot n_x \mathrm{d}S}_{\text{pressure drag}} + \underbrace{\iint_S \tau_{w,x}\mathrm{d}S}_{\text{viscous drag}}\right) \quad (2)$$

where S denotes the athlete surface, p the pressure, n_x the component of the surface normal vector in the flow direction and $\tau_{w,x}$ the component of the shear stress in the flow direction. Pressure drag is caused by a pressure difference between the front and back of the body, while viscous drag is due to friction. Since an athlete can be considered a bluff body shape, the pressure drag will dominate typically accounting for more than 95% of the total drag. The results from Eq. 2 for each individual cell were presented in a manner such that significant contributions to the total C_DA could be visualized. Furthermore, the cumulative drag as the flow passes about the skier's body was calculated by dividing the geometry

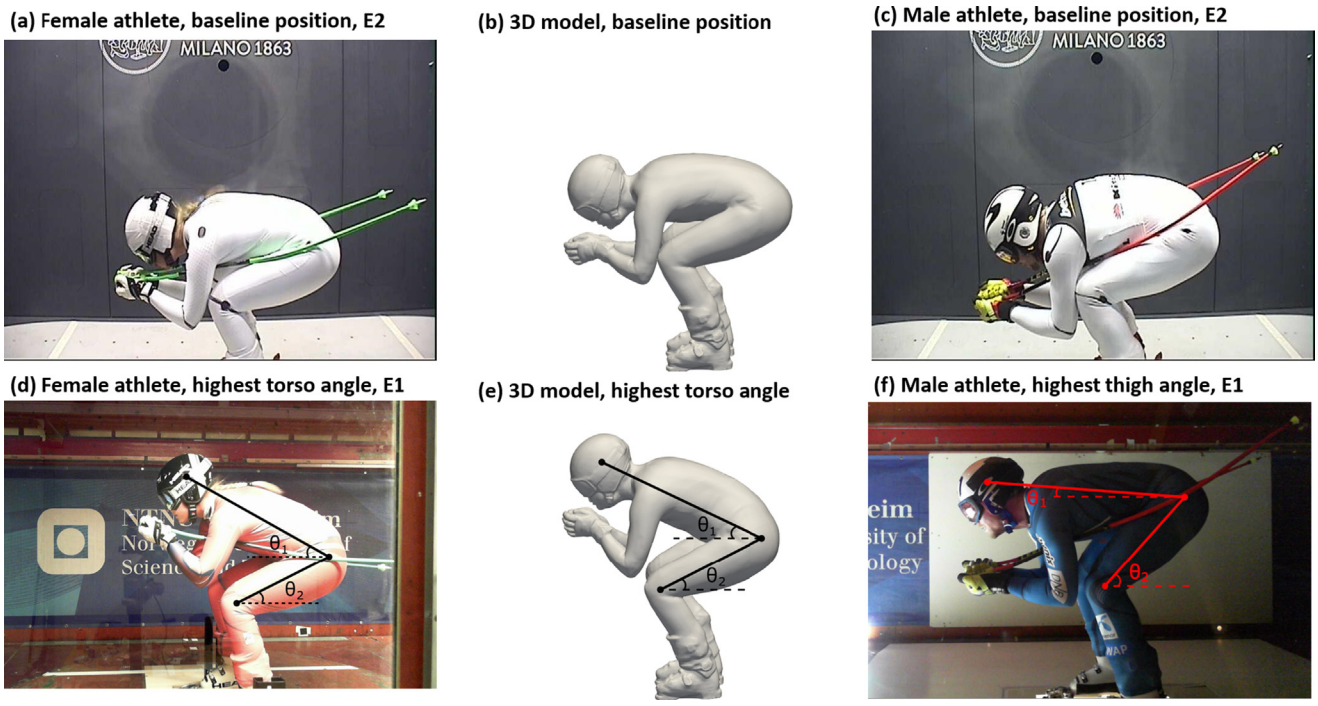

Fig. 1. Sample side-view images of the athletes and the 3D model used in the simulations, showing the definition of the torso (θ_1) and thigh (θ_2) angles in images (d)-(f).

model into bins in the flow direction and integrating the contributions of each individual bin.

3. Results

3.1. Overall flow features for the baseline model

In their baseline positions, the male and female skiers averaged (+- SD) $\theta_1 = 3.0 \pm 1.1^\circ$ and $\theta_1 = 2.9 \pm 0.8^\circ$ for the torso angle, respectively, and $\theta_2 = 31.3 \pm 0.4^\circ$ and $\theta_2 = 30.1 \pm 0.4^\circ$ for the thigh angle, respectively. Average C_DA for the baseline positions in the wind tunnel experiments were 0.184 ± 0.002 m^2 and 0.167 ± 0.002 m^2 for the male and female athlete, respectively. In the CFD simulations, a C_DA of 0.162 m^2 was measured for the female skier's baseline position, within 2–4% of her experimental values from wind tunnel testing.

Based on the cumulative development of C_DA in the simulations, the flow in the baseline position was divided into four main sections as illustrated in Fig. 2. In Section 1, C_DA increased initially as the flow first impacted the hands and helmet. This was followed by a brief reduction as the flow accelerated around the body, creating low pressure zones. C_DA then increased again as the flow separated from the hands and head, forming low-pressure wakes behind these regions. A similar but more pronounced pattern was seen in Section 2 where the flow passed over the upper arms and shoulders. As in Section 1, there was an initial sharp increase in C_DA as the flow impacted the upper arms and shoulders. This was followed by a temporary reduction as the flow accelerated around the upper arm and finally a substantial drag increase as the flow separated from the back of the upper arm. In Section 3, the flow passed over the main part of the skier's torso as well as the lower legs and boots. The torso had very little influence on C_DA development as can be seen by the lack of coloring in this region in Fig. 2. In contrast, the lower legs made a substantial impact, accounting for as much as 40–50% of the total C_DA. The initial increase and temporary reduction in drag seen on the hands and upper arms in Sections 1 and 2 was not observed in Section 3. Since the lower leg segment was angled relative to the flow,

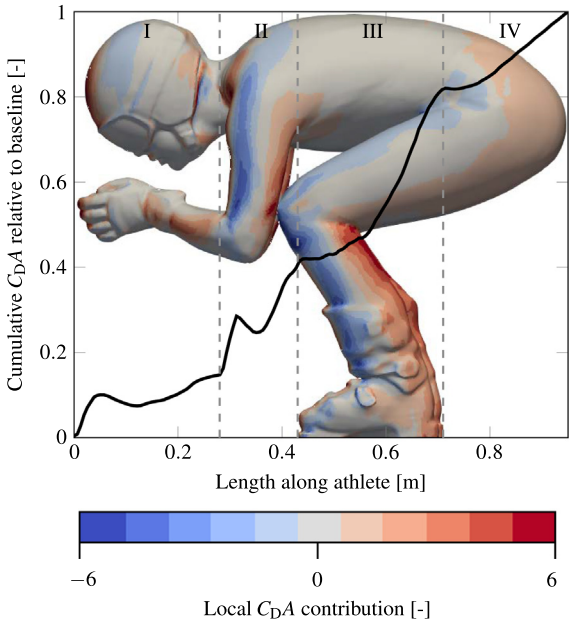

Fig. 2. Surface contour plot of C_DA contribution for the baseline position together with cumulative C_DA along the geometry model.

the initial increase and subsequent reduction of C_DA at one position on the lower leg blunted the effect of other positions giving an overall gradual increase in C_DA, before a sharp increase as the flow separated from the lower legs forming a low-pressure wake. Finally, the flow separated from the trailing end of the body in Section 4, causing a final increase in C_DA.

3.2. Influence of torso angle

Fig. 3 presents skier C_DA as a function of torso angle for both the wind tunnel (E1 and E2) and simulation results. Similar trends for

both the experimental and simulation data were observed ($\text{Trend}_{exp} = 0.78\theta_1 - 0.18$ and $\text{Trend}_{sim} = 0.79\theta_1 - 0.51$), where C_DA increased by ~0.8% per degree increase in torso angle θ_1 from baseline. The deviations for the highest tested positions were larger as these positions were difficult for the athletes to maintain during the wind tunnel testing.

Fig. 3(b) shows the surface contour plot and cumulative C_DA for the simulated position with the largest torso angle for the female athlete. The data point for this position in Fig. 3(a) is indicated by the red box. In Section 1, there was an initial increase followed by a temporary reduction in C_DA, similar to the baseline position. However, cumulative C_DA increased more in the second half of Section 1 compared to baseline, due to a greater lower arm angle and a less aerodynamic head position. In Section 2, drag area increased in a manner similar to the baseline position, although the rise was less pronounced due to the position of the lower arms. In contrast to baseline, C_DA increase in the second half of Section 2 was larger due to the position of the upper arms exposing the knees to the air flow. In Section 3, a larger increase in drag area occurred, relative to baseline, due to earlier flow separation from the back as a result of the increased torso angle. The increase in torso angle also resulted in an inclined flow separation between the legs leading to a larger wake in Section 4 and hence a larger increase in C_DA compared to the baseline position.

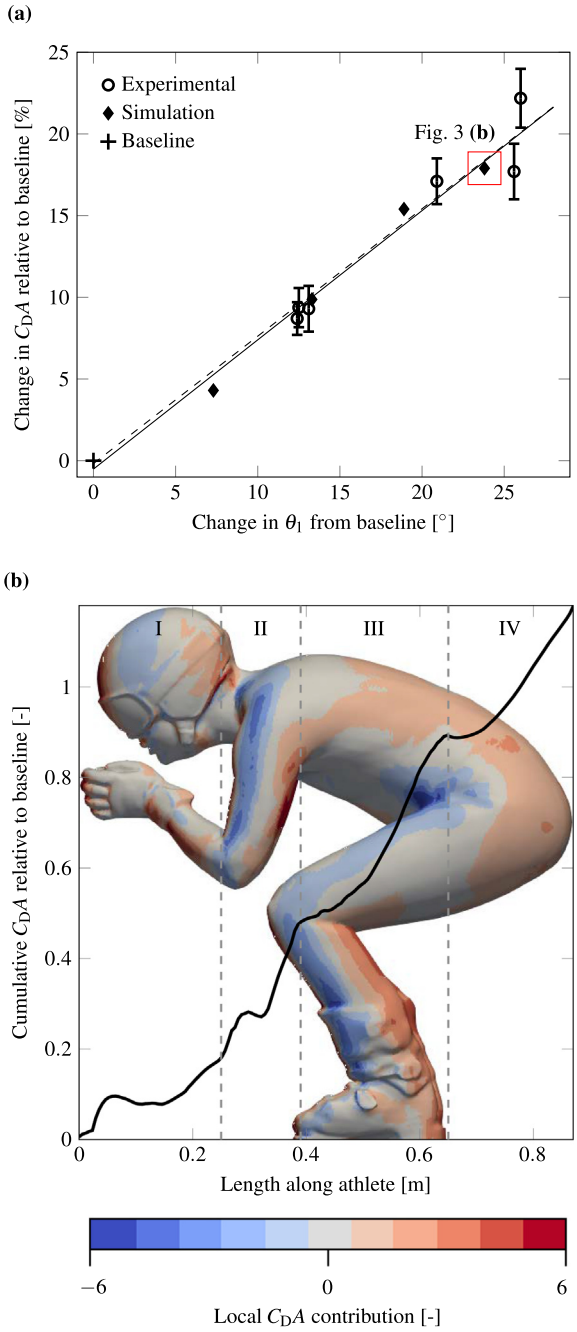

Fig. 3. (a) C_DA as a function of increased torso angle θ_1 relative to the baseline position. All experimental data can be found in Appendix A. The error bars on the experimental data points represent the standard deviation with n = 3. The dashed and fully drawn line represents the trendline of the experimental and simulated results, respectively. The red box indicates the data point corresponding to the CFD simulation results presented in (b). (b) The surface contour plot of C_DA contribution together with cumulative C_DA along the geometry model for the CFD position with the largest torso angle.

3.3. Influence of thigh angle

Fig. 4(a) presents skier C_DA as a function of thigh angle for both the experimental (E1 and E2) and simulation results. As seen for torso angle, similar trends were observed for the impact of thigh angle for both the experimental and simulation data ($\text{Trend}_{exp} = 1.18\theta_2 - 0.63$ and $\text{Trend}_{sim} = 1.20\theta_2 - 3.66$), with C_DA increasing by a slightly greater ~1.2% per degree increase in thigh angle θ_2 from baseline. Both skiers were able to maintain a constant torso angle throughout the thigh angle test series, except for the position with the highest thigh angle due to body constraints. Fig. 4(b) presents the surface contour plot and cumulative C_DA for the simulated position with the highest thigh angle for the female athlete. The data point for this position in Fig. 4(a) is indicated by a red box. The flow behaviour in both Sections 1 and 2 was similar to that of the baseline position, due to similar head and forearm positioning. C_DA remained relatively constant for the first half of Section 3 where the flow remained attached to the torso. This was followed by a sharp but small increase when the flow impacted the knees and legs. In Section 4, the flow separated from both the thighs and lower legs resulting in a large increase in C_DA, approaching ~60% of the total cumulative C_DA.

In the numerical simulations, it was found that the low tuck position could be optimized by lowering the thigh angle θ_2 from 30 ° to 20 °, resulting in a ~20% reduction in C_DA. Fig. 5 shows the cumulative drag for this position and the corresponding data point in Fig. 5(a) is indicated with a red box. The flow behavior was similar to that of the baseline position, except for the last part of Section 2 where the knees helped to fill the gaps behind the armpits in the optimized position.

In the baseline position, air flowed on the inside of the upper arm, and then exited through the gap behind the armpits and finally separated from the body. With this gap closed in the optimized position, the flow instead passed on the outside of the body and remained attached until Section 4, leading to a substantial decrease in total skier C_DA.

4. Discussion

The purpose of this investigation was to examine the aerodynamics of tucked positions in competitive alpine skiing and, in particular, to study how skier torso and thigh angle affect skier aerodynamic drag using both experimental and simulation approaches.

Looking at the cumulative drag plots in each of the analyzed positions, the role of flow separation behind the lower legs and boots in the development of drag was apparent, accounting for approximately 40–50% of the total skier drag area in the baseline positions. This finding is similar to that of Asai et al. (2016) who

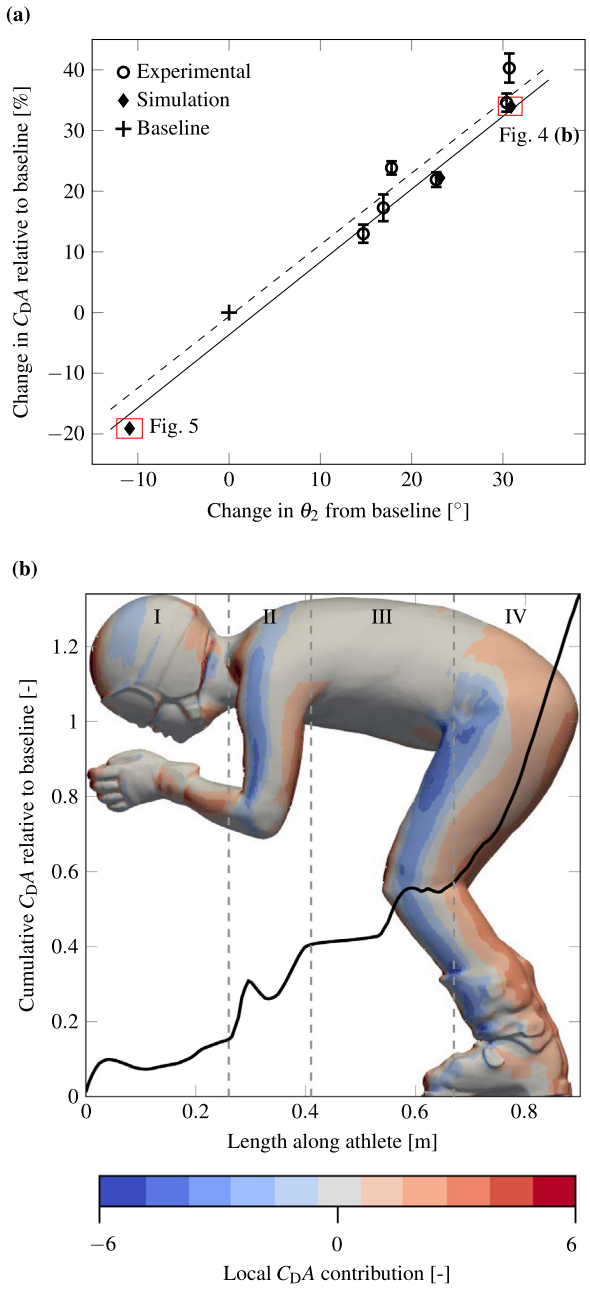

Fig. 4. (a) C_DA as a function of increased thigh angle θ_2 relative to the baseline position. All experimental data can be found in Appendix A. The error bars on the experimental data points represent the standard deviation with n = 3. The dashed and fully drawn line represents the trendline of the experimental and simulated results, respectively. The red boxes indicate the data points corresponding to the CFD simulation results presented in Figs. 4(b) and 5. (b) The surface contour plot of C_DA contribution together with cumulative C_DA along the geometry model for the CFD position with the largest thigh angle.

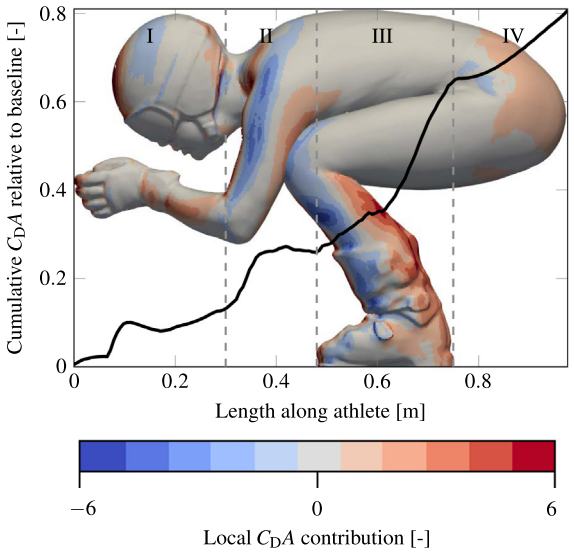

Fig. 5. Cumulative C_DA along the athlete geometry model of the female athlete for the lowest simulated thigh angle case, together with the surface contour plot of C_DA contribution along the geometry model. The corresponding data point is indicated in Fig. 4(a) with a red box.

reported that the lower legs contributed ~40% of the total drag in a tucked position. Although an alpine skier may not be able to reduce drag around the lower legs through positioning, these findings suggest that the lower legs may be an important area to consider in other drag reduction strategies such as suit design. A significant increase in drag area was also observed to originate from the upper arms (Section 2 in Fig. 2), which could be reduced by closing the gap behind the armpits with the knees in a low tuck position, as seen in Fig. 5.

Drag area increased by ~0.8% and ~1.2% per degree increased torso and thigh angle, respectively. Based on the cumulative development of drag area derived from the CFD simulations, the flow pattern in tucked positions was divided into the following four sections: (I) Hands, forearms and head; (II) shoulders, upper arms, and knees; (III) torso, thighs, lower legs, and boots; and (IV) lower back, hips, and upper thigh.

The CFD simulations revealed that while there were some minor differences in flow characteristics in Sections 1 and 2 as torso and thigh angles were increased from the baseline position, the most consequential changes in terms of drag area development occurred in Sections 3 and 4. Regarding torso angle θ_1, the simulations indicated that the main increase in drag area was associated with elevated flow separation from the lower back and torso, as torso angle increased. There was a slightly greater rate of drag area increase for the thigh segment compared to the torso, although it must be pointed out that measurements were done at higher thigh angles than torso angles to keep within realistic skiing positions. Flow simulations showed that the main increase in drag area was related to increased flow separation from the thighs in Section 4, accounting for as much as ~60% of the total drag area.

The optimized tuck position from the CFD simulations presented in Fig. 5 was of particular interest as this position was found to reduce the drag area by ~20% relative to the baseline position. The most significant difference compared to the baseline position in the optimized position was that the gaps between the armpits and knees were closed, causing the flow to remain attached in this area and consequently reducing the drag area. Some degree of individual variation and perhaps gender differences might be expected in the observed trends. However, with the limited number of subjects in this study, the influence of gender and other individual characteristics should be investigated further in future work.

This study attempted to combine both experimental and simulation methods to further our understanding of the mechanisms affecting drag development based on athlete positioning. Compared to wind tunnel studies, CFD simulations are limited in that they can not capture some important variables influencing skier drag, such as surface roughness. In addition, there is some uncertainty when validating CFD simulations due to variations in posture. However, this study focused on relative changes from baseline positions defined for both the wind tunnel tests and CFD simulations. Trends in drag area development relative to these

baseline positions were then used as the basis for analysis, to a certain degree limiting the influence of confounding variables such as surface roughness. The fact that there was a good agreement in the observed trends between the wind tunnel experiments and the simulations indicates that the overall flow pattern was sufficiently captured. However, there could be local flow features that, for instance, require an unsteady simulation or a more sophisticated treatment of surface roughness to fully capture.

In addition to the aforementioned limitations, it should be emphasized that this study focused solely on the influence of skier positioning on aerodynamics. In reality during competition, skiers must often compromise based on a number of factors. The snow surface can often be very rough, requiring the athlete to raise their position to allow for shock absorption as well as effective turning technique. Skiers must also consider how positions affect their field of vision, balance as well as the physical demands. Under these circumstances, an understanding of how each body part contributes to the overall development of aerodynamic drag can be valuable, as illustrated in this study.

5. Conclusion

In summary, this study investigated the aerodynamics of tuck positions in alpine skiing through both wind tunnel measurements and CFD simulations. The lower legs contributed approximately 40–50% of the total drag in the baseline tucked position. Drag area increased by ∼0.8% and ∼1.2% per degree increase in torso θ_1 and thigh angles θ_2, respectively. The aerodynamically best low tuck position was characterized by a torso angle θ_1 close to ∼0 ° and a low thigh angle θ_2 closing the gaps between the armpits and knees.

CRediT authorship contribution statement

Ola Elfmark: Conceptualization, Methodology, Software, Validation, Formal analysis, Resources, Writing - original draft, Writing - review & editing, Visualization, Supervision, Project administration, Funding acquisition. **Knut Erik Teigen Giljarhus:** Conceptualization, Methodology, Validation, Formal analysis, Resources, Writing - original draft, Writing - review & editing, Visualization, Supervision, Project administration. **Fredrik Fang Liland:** Software, Writing - review & editing. **Luca Oggiano:** Conceptualization, Methodology, Software, Resources, Writing - review & editing. **Robert Reid:** Conceptualization, Methodology, Formal analysis, Resources, Writing - review & editing.

Declaration of Competing Interest

The authors report no conflict of interest.

Acknowledgment

This study was carried out with support and funding from the Norwegian Olympic Committee and the Norwegian Ski Federation under the project Aerodynamics 2022. The authors would like to acknowledge and thank Ing. Stefano Giappino, Ing. Umberto Spinelli, Prof. Marco Belloli and Prof. Marco Bocciolone from the Politecnico di Milano wind tunnel for facilitating the experiment at PoliMi. The authors would also like to acknowledge the participation of the athletes who voluntarily gave their time to this research.

Appendix A. Additional wind tunnel information

A.1. Experimental setup

The wind tunnel used in E1 can produce speeds up to 25 ms^{-1}, has a cross section of 4.9 m^2 (2.7 m^2 wide and 1.8 m^2 high), has a turbulence intensity <0.24% and uses a Schenck six-component force balance to measure the drag force. The wind tunnel used in E2 can produce wind speeds up to 55 ms^{-1}, has a cross section of 15.4 m^2 (4 m^2 wide and 3.84 m^2 high), has a turbulence intensity <0.1% and uses a RUAG Aerospace six-component force balance to measure the drag force.

A.2. Blockage correction

When testing in closed wind tunnels, blockage correction should be considered when the blockage ratio is in the range of 3–10%, or higher (Battisti et al., 2011; Anthoine et al., 2009; Elfmark et al., 2020). As the male athlete had a frontal area of 0.34 m^2 in the highest torso angle tested (a blockage of ∼7% in E1), blockage correction was performed for all results in both E1 and E2. The same correction was applied for all results for consistency, even if it could have been neglected for E2 due to the small blockage ratio. Maskell's blockage correction was used in this study:

$$\frac{C_{Du}}{C_{Dc}} = 1 + \beta C_{Du}\frac{A}{CS}, \tag{A.1}$$

where C_{Du} is the uncorrected frag coefficient, C_{Dc} is the corrected drag coefficient, A the frontal area for the test subject, CS the cross section of the wind tunnel and β is an empirical blockage constant (Maskell, 1963). The blockage constant chosen for this experiment was β=1.21, suggested by Elfmark et al. when correcting for blockage on alpine skiers in high speeds (Elfmark et al., 2020).

Table A.1
Measurement data from the wind tunnel testing for the torso angle θ_1 tests (a) and the thigh angle θ_2 tests (b). These data are presented graphically in Fig. 3 and Fig. 4. + denotes the baseline position for each test.

(a) Athlete	Experiment	Change in θ_1 [°]	Rel. change in C_DA [%]
Female$^+$	E1	0	0
Female	E1	12.5	9.4±1.2
Female	E1	26.0	22.2±1.8
Female$^+$	E2	0	0
Female	E2	12.4	8.7±1.0
Female	E2	25.6	17.7±1.7
Male$^+$	E1	0	0
Male	E1	20.9	17.1±1.4
Male$^+$	E2	0	0
Male	E2	13.1	9.3±1.4
(b) Athlete	Experiment	Change in θ_2 [°]	Rel. change in C_DA [%]
Female$^+$	E1	0	0
Female	E1	17.8	23.8±1.1
Female	E1	30.7	40.3±2.4
Female$^+$	E2	0	0
Female	E2	22.7	21.9±1.2
Female	E2	30.4	34.6±1.5
Male$^+$	E1	0	0
Male	E1	16.9	17.3±2.2
Male$^+$	E2	0	0
Male	E2	14.7	13±1.5

A.3. Experimental results

The data from the different test subjects and experiments, used in Figs. 3 and 4 are presented in Table A.1.

Appendix B. Additional information on computational setup

B.1. Numerical settings and turbulence model

Simulations were performed with the k-ω SST turbulence model (Menter et al., 2003), a Reynolds-averaged Navier–Stokes turbulence model. The SIMPLE algorithm was used for pressure–velocity coupling, and second-order discretization schemes were used for spatial discretization. For the convective terms, a second-order central-upwind scheme with a Sweby limiter was used (Sweby, 1984).

B.2. Computational domain and mesh

The size of the computational domain was $20L \times 10L \times 10L$, where L is taken as the diagonal of the bounding box of the athlete geometry. This gives a blockage ratio lower than 3.0%. The geometry was placed on the ground plane, $5L$ from the inlet.

The hex-dominated unstructured mesh generator `snappyHexMesh` was used to generate the computational mesh. The total number of cells was approximately 20 million.

To ensure a suitable mesh size for the simulations, a mesh sensitivity study was performed using the baseline position geometry. The mesh was constructed as an unstructured hex-dominated mesh, with refinement near the athlete body. The cell size was increased by a factor of two across each refinement level, and a total of seven refinement levels were used. Close to the body, prism layers were inserted to resolve the sharp gradients in the boundary layer. A constant number of 20 prism layers was used for all meshes. Fig. 6 shows the overall structure of the mesh, as well as a close-up of the prism layers near the head of the athlete.

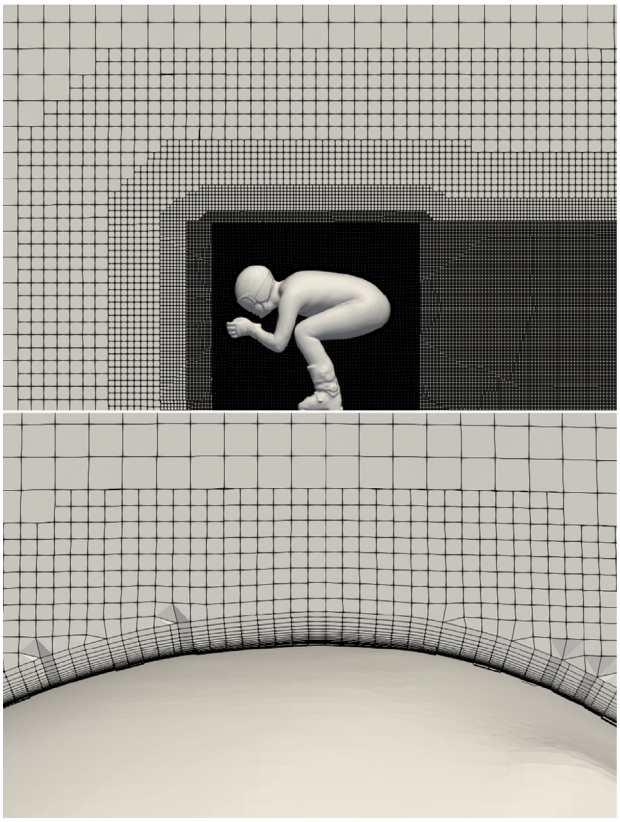

Fig. 6. Overall structure of the mesh (top) and close-up of the prism layers near the head of the athlete (bottom).

Table B.2
Information about meshes used in the mesh sensitivity study. The cell size is the size of the cell closest to the athlete body before the prism layer. Mesh size is the total number of cells in the mesh.

	Cell size [mm]	Mesh size ($\times 10^6$)	Average y^+ [–]	C_DA [m^2]
Tiny	4.10	2.22	22.3	0.1577
Coarse	3.35	7.94	3.85	0.1570
Medium	2.80	12.7	2.88	0.1601
Fine	2.33	20.1	2.17	0.1616
Extra fine	1.94	32.3	1.73	0.1618
Ultra fine	1.61	54.6	1.40	0.1616

The mesh sequence was made by successively increasing the number of cells in each direction of the base mesh by a factor of 20%. Table B.2 gives a summary of the meshes used and the resulting C_DA, where "Cell size" denotes the size of the cells in the finest grid level near the athlete geometry, before the prism layer. The mesh shown in Fig. 6 is the fine mesh referenced in Table B.2. As the mesh is refined, the C_DA stabilizes around a value of $C_DA \approx 0.162$. Although full mesh convergence was not achieved, the fine mesh was chosen for the simulations in this work since the changes in C_DA were small when the grid was refined further.

B.3. Boundary conditions

The experiments presented in this work were done at speeds ranging from 25 ms^{-1} and 35 ms^{-1}. To save computational time, a lower speed of 20 ms^{-1} was chosen for the simulations. Since we fully resolve the boundary layers and due the choice of meshing software, the number of grid points needed near the athlete body scale linearly with the flow velocity to maintain the same non-dimensional distance to the wall. For instance, a 50% decrease of grid cell size is necessary to go from 20 ms^{-1} to 30 ms^{-1}. This yields a 3.375$\times$ increase in total grid cells, from 20 million to 70 million cells. As a test of the relative difference between positions at these two speeds, CFD simulations were performed with a 50% increase in speed for the baseline position and the position with maximum torso angle. The increase in drag from the baseline position to the position with high torso angle was 18.63% for the simulation speed used in this work. For the higher speed, the increase was 18.87%, which gives a difference of only 0.24%. Additionally, Elfmark et al. (2020) found similar results for the C_DA for a downhill skier at 20 ms^{-1} and 30 ms^{-1}, further justifying the use of a lower simulation speed.

The inlet boundary was given a uniform constant velocity, with zero gradient for pressure. Low turbulence levels were assumed, consistent with the wind-tunnel experiments, with a turbulent intensity of 0.5%. At the outlet, a fixed pressure was set with zero gradient for the remaining variables. The sides of the domain used a slip boundary condition. For the athlete and ground, a no-slip boundary condition with zero roughness and a wall function blending between the viscous sublayer and the log-law region was applied (Spalding, 1961). In bluff-body flow, the transition from laminar to turbulent flow in the boundary layer can be crucial to estimate the correct flow separation point. In this work, the boundary layer is always assumed to be turbulent. This has been shown to give good results past the critical point (Ong et al., 2009). This is also an additional reason for why a lower speed

can be selected for the modelling, as the simulations will show supercritical behavior earlier than the experiments as demonstrated by Sørensen et al. (2011) for flow over a cylinder.

References

Anthoine, J., Olivari, D., Portugaels, D., 2009. Wind-tunnel blockage effect on drag coefficient of circular cylinders. Wind Struct. 12 (6), 541–551.

Asai, T., Hong, S., Ijuin, K., 2016. Flow visualization of downhill ski racers using computational fluid dynamics. Procedia Eng. 147, 44–49.

Barelle, C., Ruby, A., Tavernier, M., 2004. Experimental model of the aerodynamic drag coefficient in alpine skiing. J. Appl. Biomech. 20 (2), 167–176.

Battisti, L., Zanne, L., Dell'Anna, S., Dossena, V., Persico, G., Paradiso, B., 2011. Aerodynamic measurements on a vertical axis wind turbine in a large scale wind tunnel. J. Energy Resources Technol. 133 (3).

Blocken, B., Toparlar, Y., 2015. A following car influences cyclist drag: CFD simulations and wind tunnel measurements. J. Wind Eng. Ind. Aerodyn. 145, 178–186.

Blocken, B., Defraeye, T., Koninckx, E., Carmeliet, J., Hespel, P., 2013. CFD simulations of the aerodynamic drag of two drafting cyclists. Comput. Fluids 71, 435–445.

Blocken, B., Toparlar, Y., Andrianne, T., 2016. Aerodynamic benefit for a cyclist by a following motorcycle. J. Wind Eng. Ind. Aerodyn. 155, 1–10.

Brownlie, L., 2020. Aerodynamic drag reduction in winter sports: The quest for "free speed". Proc. Inst. Mech. Eng., Part P: J. Sports Eng. Technol. https://doi.org/10.1177/1754337120921091.

Brownlie, L., Larose, G., D'Auteuil, A., Allinger, T., Meinert, F., Kristofic, P., Dugas, S., Boyd, R., Stephens, D., 2010. Factors affecting the aerodynamic drag of alpine skiers. Procedia Eng. 2 (2), 2375–2380.

Chen, Z., Fang, H., 2011. The effects of wind and posture on the aerodynamic performance during the flight stage of skiing. J. Biomech. Eng. 133 (9), 091001.

Defraeye, T., Blocken, B., Koninckx, E., Hespel, P., Carmeliet, J., 2010. Aerodynamic study of different cyclist positions: CFD analysis and full-scale wind-tunnel tests. J. Biomech. 43 (7), 1262–1268.

Elfmark, O., Bardal, L.M., 2018. An empirical model of aerodynamic drag in alpine skiing. In: Multidisciplinary Digital Publishing Institute Proceedings, vol. 2, p. 310.

Elfmark, O., Reid, R., Bardal, L.M., 2020. Blockage Correction and reynolds number dependency of an alpine skier: a comparison between two closed-section wind tunnels. In: Multidisciplinary Digital Publishing Institute Proceedings, vol. 49, p. 19.

Gardan, N., Schneider, A., Polidori, G., Trenchard, H., Seigneur, J.-M., Beaumont, F., Fourchet, F., Taiar, R., 2017. Numerical investigation of the early flight phase in ski-jumping. J. Biomech. 59, 29–34.

Giljarhus, K.E.T., Stave, D.Å., Oggiano L., 2020. Investigation of influence of adjustments in cyclist arm position on aerodynamic drag using computational fluid dynamics. In: Multidisciplinary Digital Publishing Institute Proceedings, vol. 49, p. 159.

Jasak, H., Jemcov, A., Tukovic, Z., et al., 2007. OpenFOAM: A C++ library for complex physics simulations. In: International Workshop on Coupled Methods in Numerical Dynamics, vol. 1, pp. 1–20.

Maskell, E., 1963. A theory of the blockage effect on bluff bodies and stalled wings in a closed wind tunnel. Tech. Rep., Aeronautical Research Council London (United Kingdom).

Meile, W., Reisenberger, E., Mayer, M., Schmölzer, B., Müller, W., Brenn, G., 2006. Aerodynamics of ski jumping: experiments and cfd simulations. Exp. Fluids 41 (6), 949–964.

Menter, F.R., Kuntz, M., Langtry, R., 2003. Ten years of industrial experience with the SST turbulence model. Turbulence, Heat Mass Transfer 4 (1), 625–632.

Meyer, F., Le, D.P., Borrani, F., 2012. Aerodynamic drag modeling of alpine skiers performing giant slalom turns. Med. Sci. Sports Exercise 44 (6), 1109–1115.

Nørstrud, H., Øye, I., 2009. On cfd simulation of ski jumping. In: Computational Fluid Dynamics for Sport Simulation. Springer, pp. 63–82.

Oggiano, L., Spurkland, L., Sætran, L., Bardal, L.M., 2015. Aerodynamical Resistance in Cycling on a Single Rider and on Two Drafting Riders: CFD Simulations, Validation and Comparison with Wind Tunnel Tests. In: International Congress on Sports Science Research and Technology Support, pp. 22–37.

Ong, M.C., Utnes, T., Holmedal, L.E., Myrhaug, D., Pettersen, B., 2009. Numerical simulation of flow around a smooth circular cylinder at very high Reynolds numbers. Marine Struct. 22 (2), 142–153.

Savolainen, S., Visuri, R., 1994. A review of athletic energy expenditure, using skiing as a practical example. J. Appl. Biomech. 10 (3), 253–269.

Sørensen, N.N., Bechmann, A., Zahle, F., 2011. 3D CFD computations of transitional flows using DES and a correlation based transition model. Wind Energy 14 (1), 77–90.

Spalding, D.B., 1961. A single formula for the law of the wall. J. Appl. Mech. 28 (3), 455–458.

Supej, M., Sætran, L., Oggiano, L., Ettema, G., Šarabon, N., Nemec, B., Holmberg, H., 2013. Aerodynamic drag is not the major determinant of performance during giant slalom skiing at the elite level. Scandinavian J. Med. Sci. Sports 23 (1), e38–e47.

Sweby, P.K., 1984. High resolution schemes using flux limiters for hyperbolic conservation laws. SIAM J. Num. Anal. 21 (5), 995–1011.

Watanabe, K., Ohtsuki, T., 1977. Postural changes and aerodynamic forces in alpine skiing. Ergonomics 20 (2), 121–131.

Weller, H.G., Tabor, G., Jasak, H., Fureby, C., 1998. A tensorial approach to computational continuum mechanics using object-oriented techniques. Comput. Phys. 12 (6), 620–631.

WMA, 2001. World Medical Association Declaration of Helsinki. Ethical principles for medical research involving human subjects. Bull. World Health Organ. 79 (4), 373.